INVITED PAPER

Plasmons in Graphene: Fundamental Properties and Potential Applications

In graphene, plasmons are expected to provide valuable insights into many-body effects that include electron–phonon, electron–electron, and plasmon–phonon interactions. This paper provides a critical review of the state of research in this area.

By Marinko Jablan, Marin Soljačić, and Hrvoje Buljan

ABSTRACT | Plasmons in graphene have intriguing fundamental properties and hold great potential for applications. They enable strong confinement of electromagnetic energy at subwavelength scales, which can be tuned and controlled via gate voltage, providing an advantage for graphene's plasmons over surface plasmons (SPs) on a metal–dielectric interface. They have been described for a large span of frequencies from terahertz up to infrared and even in the visible. We provide a critical review of the current knowledge of graphene plasmon properties (dispersion and linewidth) with particular emphasis on plasmonic losses and the competition between different decay channels, which are not yet fully understood. Plasmons in graphene provide an insight into interesting many-body effects such as those arising from the electron–phonon interaction and electron–electron interactions, including hybrid plasmon–phonon collective excitations (either with intrinsic or substrate phonons) and plasmarons. We provide a comparison of SPs on a metal–dielectric interface with plasmons in graphene and 2-D metallic monolayers. We finally outline the potential for graphene's plasmons for applications.

KEYWORDS | Graphene; nanophotonics; plasmons; propagation losses

I. INTRODUCTION

Recent years have witnessed a tremendous progress in the planar waveguide and photonic crystals technology, which paves the way toward novel, more efficient, and miniaturized optical devices. Photonic elements can operate at hundreds of terahertz (THz) frequencies with large bandwidths and low losses, thus surpassing the gigahertz (GHz) frequencies and bandwidth limits of the electronic devices. However, the spatial limitation for the size of optical devices is the diffraction limit, that is, the wavelength of light, which is at best on the order of a micrometer, whereas electronic devices are miniaturized to the nanoscale. To scale optical devices down to these ultimate limits for the fabrication of highly integrated nanophotonic devices, that could operate at near-infrared (IR) or visible frequencies with large bandwidths, requires confinement and control of electromagnetic energy well below the diffraction limit. One and perhaps the only viable path toward such nanophotonic devices are plasmonic excitations that are within the focus of a growing field of research: plasmonics [1]–[4].

In nature, there are versatile types of plasmonic excitations depending on the geometry and dimensionality of the system. Bulk plasmons are collective excitations of electrons in conductors, however, they are not very interesting from the point of view of photonics. Plasmonics is founded on surface-plasmon polaritons [or simply surface plasmons (SPs)]—electromagnetic (EM) waves trapped at the conductor–dielectric interface due to collective surface excitations of carriers [1]–[3]. Their wavelength is much

Manuscript received December 20, 2012; revised April 22, 2013; accepted April 22, 2013. Date of publication May 23, 2013; date of current version June 14, 2013. This work was supported in part by the Croatian Ministry of Science under Grant 119-0000000-1015 and Unity through Knowledge Fund Grant Agreement 93/11. The work of M. Soljačić was supported in part by the MIT S3TEC Energy Research Frontier Center of the Department of Energy under Grant DE-SC0001299. This work was also supported in part by the Army Research Office through the Institute for Soldier Nanotechnologies under Contract W911NF-07-D0004, as well as by the MRSEC program of the National Science Foundation under Award DMR-0819762.
M. Jablan and **H. Buljan** are with the Department of Physics, University of Zagreb, 10000 Zagreb, Croatia (e-mail: mjablan@phy.hr; hbuljan@phy.hr).
M. Soljačić is with the Department of Physics, Massachusetts Institute of Technology, Cambridge, MA 02139 USA (e-mail: soljacic@mit.edu).
Digital Object Identifier: 10.1109/JPROC.2013.2260115

smaller than the wavelength of the light in air at the same frequency, which enables control of light at the nanoscale, thereby breaking the diffraction limit [1]–[4]. This possibility has also led to the investigation of plasmons in 2-D electron gases found in various types of materials, including inversion layers [5], heterostructures [6], and monoatomic metallic layers [7]–[9]. However, the search for better plasmonic materials with greater confinement of the electromagnetic energy and lower losses is still underway [3]. The advent of graphene with its extraordinary electric, optical, and mechanical properties has in recent years opened up a whole new avenue of research on plasmons in graphene, which is reviewed in this paper.

Graphene is a 2-D sheet of carbon atoms arranged in a honeycomb lattice [10]–[12], which was demonstrated to have extraordinary electric properties [10]–[16], such as extremely large mobilities. It can be doped to high values of electron or hole concentrations by applying external gate voltage [10], which has a dramatic effect on its optical properties [17], [18]. This is a great motivation for investigating graphene in the context of optical and plasmonic applications. Moreover, it can be successfully placed on top of versatile substrates such as dielectrics and metals, but also suspended in air.

Plasmons in graphene have attracted considerable attention in recent years, both in the experimental [19]–[30] and theoretical arenas [31]–[67]. One of the main reasons for this is a fact that their properties such as dispersion and intraband losses via excitation of electron–hole pairs can be tuned by external gate voltage (thereby increasing/decreasing the concentration of carriers).

Experimental evidence for the existence of plasmonic effects in graphene was first obtained with electron energy-loss spectroscopy (EELS) [19]–[21]. However, excitation of plasmons with optical means and the studies of optical phenomena with graphene plasmons have been within the focus of several exciting recent experiments [22]–[29]. Because the wavevector of the plasmons in extended monolayer graphene is much larger than the wavevector of the freely propagating photons, the coupling of light to plasmons has to somehow overcome this mismatch. Infrared nanoscopy and nanoimaging experiments confine IR light onto a nanoscale tip enabling an increase of the in-plane component of the momentum, which enables optical excitation of plasmons [23]–[25] and their imaging in real space [24], [25]. Patterned graphene structures, ribbons [22], disks [26], [29], or rings [27], organized in a periodic superlattice, break translational invariance and enable optical excitation of plasmons with free propagating incident light. Such systems have already demonstrated the possibility of constructing plasmonic devices [26], [27]. Particularly intriguing excitations are magnetoplasmons in graphene [28], [29]: plasmons occurring in the presence of the magnetic field which changes electronic band structure (introduces Landau levels), and leads to interesting phenomena such as prolongation of lifetime of edge magnetoplasmons in disks with the increase of the magnetic field [29]. Also noteworthy is the possibility of atomically localized plasmon enhancement in monolayer graphene observed with EELS in an aberration-corrected scanning transmission electron microscope (STEM) [30].

There are numerous studies of graphene plasmons on the theoretical side [31]–[67]. Some of those investigate plasmons from the fundamental point of view are: their dispersion [32], [33], their interaction with other excitations in graphene (thereby investigating many-body effects such as plasmon–phonon coupling [39], [40] and plasmarons [41]), their losses from various scattering mechanisms [38], interactions with a magnetic field [51]–[53], and modifications under strain [54], [55]. A number of studies are aimed at patterned structures such as ribbons and disks where finite size effects and boundary conditions are important, which yields numerous plasmonic phenomena and opens up the way to design versatile devices.

Let us outline some of the theoretically proposed phenomena and applications involving plasmons in graphene that this review draws upon. Plasmons can couple to other elementary excitations in graphene yielding versatile many-body effects. Plasmon–phonon collective excitations can occur either by coupling with surface phonons of a polar substrate [39], or with intrinsic optical phonons of graphene [40]. Collective excitations of charge carriers and plasmons, referred to as plasmarons, have been recently addressed [41] in the context of near-field optics [24], [25]. It was suggested that illuminating graphene with circularly polarized light gives rise to an energy gap between the conduction and the valence bands; this system supports collective plasma excitations of optically dressed Dirac electrons [42]. A particularly important question is that of electron–electron interaction on plasmons beyond the random phase approximation (RPA) [43], [44]. The recombination rates of carriers due to plasmon emission were predicted to range from tens of femtoseconds to hundreds of picoseconds, with sensitive dependence on the system parameters [45].

Graphene plasmons have attracted interest also in the context of near-field enhancement, i.e., systems where a great amount of electromagnetic energy is confined at subwavelength scales. A particularly interesting system in this context is a nanoemitter (oscillating dipole) in the vicinity of the graphene sheet [46]–[48], which can efficiently excite plasmons and lead to strong light–matter interactions and quantum effects. Near-field enhancement has been predicted in a periodically gated graphene with a defect [49], while the existence of plasmon modes in a double-layer graphene structure leads to near-field amplification [50].

An interesting avenue of research is strain engineering the properties of graphene and its excitations, which is possible due to its extraordinary mechanical properties.

Polarization of graphene and plasmons under strain have been investigated in [54] and [55].

Plasmons in graphene with a magnetic field present have also attracted theoretical interest [51]–[53]: the dependence of their properties such as dispersion has been studied in dependence of the magnetic field.

Nonlinear optical phenomena are of particular interest, given the fact that considerable electromagnetic energy can be confined to small volumes in graphene. It has been pointed out that quantum effects can introduce a strong nonlinear optical response in a system formed by a doped graphene nanodisk and a nearby quantum emitter, which yields the plasmon blockade effect (analogous to Coulomb or photon blocade effects) [56]. However, in contrast to photon blockade, the wavelength at which plasmon blockade takes place can be tuned simply by electrostatic gating [56]. A paradigmatic nonlinear phenomenon—second harmonic generation—was predicted to be strongly plasmon enhanced in graphene [57].

Finally, graphene plasmons have been proposed for applications in versatile types of devices. Graphene holds a great promise in the context of so-called transformation optics [58], because different parts of the sheet can be gated by different voltages yielding a platform for transformation optical devices (e.g., plasmon Fourier optics [59]). Graphene plasmon waveguides in single and paired nanoribbon structures were analyzed [61], and guided plasmons in graphene p–n junctions were considered [62]. Moreover, coherent terahertz sources based on plasmon amplification were suggested [63], [36]. In optically pumped graphene structures (out of equilibrium conditions), amplification of terahertz plasmons was predicted [64]. Optical response (due to plasmons) in periodically patterned structures made of graphene disks was predicted to yield 100% absorption [65]. Tunable terahertz optical antennas based on graphene ring structures were proposed [60].

Besides the usual transverse magnetic plasmons, graphene was predicted to support a transverse electric (TE) mode [35], which is not present in usual 2-D systems with parabolic electron dispersion. This mode resides very close to the light line [40] and, therefore, does not seem to be so interesting for confinement of electromagnetic energy. In a bilayer graphene [67], the confinement is somewhat stronger, but dispersion is still very close to the light line.

The outline of this review is as follows. In Section II, we present the basic concepts related to plasmons in general and plasmons in graphene. This section is intended to be pedagogical, for the newcomers to this field. In Section III, we discuss plasmons in patterned graphene structures, both experiments and theory. In Section IV, we review recent studies on plasmons in graphene performed via infrared nanoscopy and nanoimaging [23]–[25]. In Section V, we focus on many-body effects and losses of graphene plasmons. We discuss possible channels of decay, estimated decay rates for these channels, and open questions. In Section VI, we discuss plasmons in metallic monolayers and provide a comparison of these systems with graphene. In Section VII, we discuss other directions of research related to graphene plasmons, and finally we conclude.

II. BASIC CONCEPTS

As we already mentioned in the introduction, SPs polaritons are electromagnetic (EM) waves trapped at a surface of conductor [1]–[4]. Let $x = 0$ define a surface between metal with dielectric function $\epsilon(\omega)$ and dielectric with dielectric constant ϵ_r. Under certain conditions, this system can support EM wave of frequency ω that propagates along the surface of metal with wavevector q, while EM fields decay exponentially away from the surface. If we write for the electric and magnetic fields $F(x > 0) \propto e^{-Kx}$ above the metal, and $F(x < 0) \propto e^{K_m x}$ in the metal, then elementary electrodynamics [71] requires that $K = \sqrt{q^2 - \epsilon_r \omega^2/c^2}$ and $K_m = \sqrt{q^2 - \epsilon(\omega)\omega^2/c^2}$. By matching the boundary conditions, for the case of transverse magnetic (TM) polarization, we find the dispersion relation

$$1 = -\frac{\epsilon(\omega)}{\epsilon_r}\frac{K}{K_m}. \tag{1}$$

Here, we see that the required condition is $\epsilon(\omega) < 0$, which is why metals are usually used, but polar materials can sustain a similar kind of modes (termed surface-phonon polaritons [72], [73]). Equation (1) can be solved to give an explicit expression for the dispersion relation

$$q = \frac{\omega}{c}\sqrt{\frac{\epsilon_r \epsilon(\omega)}{\epsilon_r + \epsilon(\omega)}} \tag{2}$$

which is shown in Fig. 1. From (2), we see that for a characteristic frequency, i.e., when $\epsilon(\omega) = -\epsilon_r$, wavevector diverges $q \gg \omega/c$; i.e., at the certain frequency, the SP wavelength is much smaller than the corresponding wavelength of light in free space. This is in fact arguably the most interesting characteristic of SPs since they enable confinement of EM waves significantly below the diffraction limit. On the other hand, note that in this regime $K \approx K_m \approx q$, which means that the fields are also squeezed to a subwavelength regime perpendicular to the interface and can be significantly enhanced for a given pulse energy.

Let us imagine now a thin metal slab of thickness d and see what happens when we decrease d (see also supporting material from [58]). SPs from two surfaces can now couple and form even and odd TM mode but only the latter one

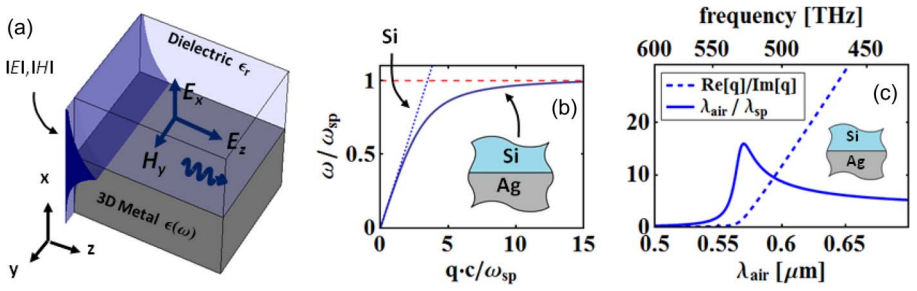

Fig. 1. *(a) Schematic description of an SP on metal–dielectric interface. (b) SP dispersion curve (solid blue line) for Ag–Si interfaces; dotted blue is the light line in Si (dispersion relation of light in bulk Si); dashed red line denotes the SP resonance. (c) Wave localization (solid line) and propagation length (dashed line) for SPs at Ag–Si interface (experimental Ag losses are taken into account).*

survives in the $d \to 0$ limit. The corresponding dispersion relation is

$$\frac{e^{K_m d}+1}{e^{K_m d}-1} = -\frac{\epsilon(\omega)}{\epsilon_r}\frac{K}{K_m}. \tag{3}$$

Let us now write the metal dielectric function as $\epsilon(\omega) = 1 + (i\sigma_v(\omega)/\omega\epsilon_0)$. Here $\sigma_v(\omega)$ is the volume conductivity of the metal in question so that the volume current density is given by $\mathbf{J}_v = \sigma_v \mathbf{E}$. In the case of a thin slab $(d \cdot K_m \ll 1)$, EM fields and induced currents are essentially uniform across the slab, and we can introduce the effective surface current density $\mathbf{J}_s = \mathbf{J}_v \cdot d$. If we require $\mathbf{J}_s = \sigma_s \mathbf{E}$, the appropriate surface conductivity is $\sigma_s = \sigma_v \cdot d$, and in this limit $(d \cdot K_m \ll 1)$, we obtain dispersion relation [58]

$$K = \frac{2i\omega\epsilon_0\epsilon_r}{\sigma_s(\omega)}. \tag{4}$$

Note that the identical expression is obtained [35] for TM EM wave trapped at 2-D sheet of charges described by a surface conductivity $\sigma_s(\omega)$, in which electron response is frozen perpendicular to the plane. However, in that case, it would be more common to use the term plasmon polaritons, because it describes self-consistent collective oscillation of electrons in a 2-D system [33]. By looking at the same problem from a different perspective, one could also conveniently model this 2-D system with a thin slab of corresponding bulk dielectric function [58] $\epsilon(\omega) = 1 + (i\sigma_s(\omega)/\omega\epsilon_0 d)$, as long as the condition $d \cdot K_m \ll 1$ is satisfied.

To get a better sense of SP modes let us assume that the metal is described by a Drude model, which is an excellent approximation for most metals up to the onset of interband absorption [68]. In that case, we can write

$$\sigma_v(\omega) = \frac{n_v e^2}{m^*}\frac{i}{\omega + i/\tau} \tag{5}$$

where m^* is the effective electron mass, τ is the relaxation time, and n_v is the electron volume density. The surface conductivity (σ_s) can be obtained from the same expression by simply changing n_v into the effective electron surface density $n_s = n_v \cdot d$. If we neglect the damping term $(\tau \to \infty)$ for the moment, we can write the dielectric function in the Drude model as $\epsilon(\omega) = 1 - \omega_p^2/\omega^2$, where $\omega_p = n_v e^2/\epsilon_0 m^*$ is the frequency of volume plasma oscillations. Then, the dispersion relation (frequency versus wave vector) for an SP at a single metal surface (semi-infinite metal) asymptotically approaches the value $\omega = \omega_p/\sqrt{1+\epsilon_r}$, which satisfies the condition $\epsilon(\omega) = -\epsilon_r$ [see (2)]. Note that, even though they are both similar in frequency, bulk plasmon and SP are qualitatively very different. The former one is described by a bulk oscillation of charge density, while the latter one involves only oscillation of surface charge density with EM fields that are localized to the metal surface.

For the case of a thin metal slab, we have more complicated behavior, and (4) gives us

$$q = \frac{2m^*\epsilon_0\epsilon_r}{n_s e^2}\omega(\omega + i/\tau) \tag{6}$$

where the effective electron surface density is $n_s = n_v \cdot d$, and we took $K \approx q$, since we are mostly interested in the electrostatic limit $(q \gg \omega/c)$. However, for sufficiently large wave vectors, when $d \cdot K_m \ll 1$ is no longer valid, SPs from two surfaces decouple, and we are left with the bare SP dispersion from (2).

Note that (4) and (6) are valid in the extreme case of a one-atom-thick metallic layer. Nevertheless, the case of a few atomic layers is substantially more complicated since the electronic wave functions across the slab get quantized. This results in the emergence of electronic subbands and intersubband transitions, which modify the plasmon dispersion [8], [9], [70].

There is one significant advantage of using monolayers over the bulk materials since the former can be simply

influenced electrostatically. When bulk metal is connected to some electrostatic potential, electrons arrange themselves along the surface of the metal and uniformly shift all the electron states inside the bulk [68]. However, that does not change the Fermi level relative to the band minimum so the volume density of electrons and metal dielectric function remain unchanged. In contrast, in the case of a single surface of monolayer crystal, the additional surface electrons actually change the Fermi level: this changes the surface conductivity, and correspondingly the optical response of the system.

We defer the analysis of metallic monolayers to Section VI, and focus our attention until then to a special kind of one-atom-thick crystal called graphene. Graphene indeed deserves a special attention due to its extraordinary mechanical stability: graphene was shown to exist even in the suspended samples, while metallic monolayers were only demonstrated to exist on substrates which play a significant role in stabilizing their structure.

Graphene is a 2-D crystal of carbon atoms arranged in a honeycomb structure. The electron band structure is easily derived from a tight binding model, which results in peculiar Dirac cones which touch at the corners of the Brillouin zone [74]. Near these points, electron dispersion is described by a linear relation $E_n(p) = nv_F p$, where $E\ (p)$ stands for electron energy (momentum), $v_F = 10^6$ m/s is the Fermi velocity, and $n = 1$ $(n = -1)$ stands for conduction (valence) band. Note that this is very different from the usual parabolic electron dispersion encountered in metals described by $E(p) = p^2/2m^*$. Intrinsic graphene does not have free carriers since valence and conduction bands touch at the Fermi level. Nevertheless, it can be doped and, as such, it can sustain surface modes described by (4). Moreover, due to this finite doping, Pauli principle will block some of the interband transitions, allowing for existence of well-defined surface modes. Therefore, for large doping (i.e., small plasmon energies), we can use a semiclassical model [68] to describe behavior of our system. This is a generalization of the Drude model for the case of arbitrary band structure: in graphene, doped to n_s electrons per unit area, we obtain surface conductivity

$$\sigma_D(\omega) = \frac{e^2 v_F \sqrt{n_s}}{\sqrt{\pi}\hbar} \frac{i}{\omega + i\tau^{-1}}. \tag{7}$$

Equation (4) implies that the plasmon dispersion in the electrostatic limit is

$$q = \frac{2\hbar\sqrt{\pi}\epsilon_0\epsilon_r}{v_F\sqrt{n_s}e^2}\omega(\omega + i/\tau). \tag{8}$$

For larger plasmon energies, we have to take into consideration interband transitions, which can be derived from a Fermi golden rule. The corresponding part in the conductivity is [75]

$$\sigma_I(\omega) = \frac{e^2}{4\hbar}\left(\theta(\hbar\omega - 2E_F) - \frac{i}{\pi}\ln\left|\frac{2E_F + \hbar\omega}{2E_F - \hbar\omega}\right|\right) \tag{9}$$

where E_F is the Fermi level, and we are working in low-temperature/high-doping limit (i.e., $E_F \gg kT$), which is also true for (7). The total conductivity is now simply $\sigma_s(\omega) = \sigma_D(\omega) + \sigma_I(\omega)$. Note that now in a small interval for frequencies below $2E_F$, the imaginary part of the conductivity is negative $(\Im\sigma(\omega) < 0)$ and (4) does not have a solution, so graphene does not support this kind of transverse magnetic surface modes. On the other hand, it can be shown that, in this frequency, interval graphene supports TE surface modes, which can be obtained as the limiting case of a guided TE mode in a thin $(d \to 0)$ high-index dielectric waveguide [58]. It is straightforward to show that the dispersion relation of this TE mode is given by [58]

$$K = \frac{\mu_0\omega i\sigma_s(\omega)}{2}. \tag{10}$$

Compare this to (4) and note that (10) requires a different sign of imaginary part of conductivity.

One can also notice from (9) that the real part of the interband conductivity has a finite value for frequencies above $2E_F$ indicating a loss process. This was indeed verified experimentally in [69], where it was demonstrated that graphene absorbs about 2% of normal incidence light, which is quite an astonishing result since graphene is a single atom thick material. In this absorption process, the incident photon excites an electron from the valence to the conduction band, and due to the peculiar linear band dispersion, this absorption is frequency independent. Of course, for a finite doping, Pauli principle blocks transitions for photon energies below $2E_F$.

An identical process of electron–hole excitation leads to plasmon damping. However, from (8), we see that plasmon has a finite wave vector, which changes the interband transitions but also allows plasmon to excite electron–hole pair within a single band (intraband excitation). Conservation of energy and momentum requires for these transitions to obey $\hbar\omega_p(\mathbf{q}) = E_{n'}(\mathbf{p} + \hbar\mathbf{q}) - E_n(\mathbf{p})$. In this case, like before, for finite doping $E_F > 0$, Pauli principle blocks interband transitions $(n = -1, n' = 1)$ for plasmon energies $\hbar\omega_p(\mathbf{q}) < 2E_F - \hbar v_F q$, and intraband transitions $(n = n' = 1)$ for energies $\hbar\omega_p(\mathbf{q}) > \hbar v_F q$. On the other hand, outside this triangle [see Fig. 2(c)], plasmon experiences large damping due to electron–hole excitations. To

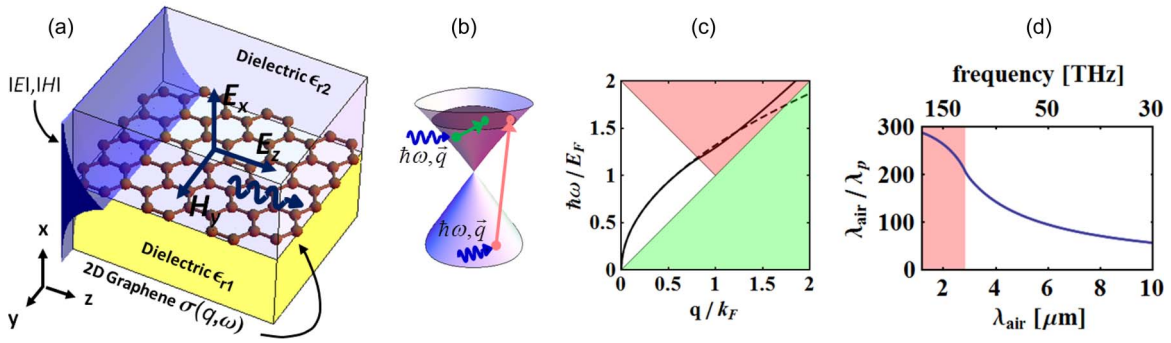

Fig. 2. *(a) Schematic of the graphene system and TM plasmon modes. Note that the profile of the EM fields looks the same as the fields of an SP [Fig. 1(a)]. (b) Sketch of the intraband (green arrows) and interband (red arrows) single particle excitations that can lead to large losses; these losses can be avoided by implementing a sufficiently high doping. (c) Plasmon RPA (solid line) and semiclassical (dashed line) dispersion curves for graphene overlaid on top of a SiO_2 ($\epsilon_{r1} = 4$ and $\epsilon_{r2} = 1$). The green (lower) and rose (upper) shaded areas represent regimes of intraband and interband excitations, respectively. (d) Localization parameter λ_{air}/λ_p.*

describe plasmon behavior for large wave vectors, one needs to resort to nonlocal theory and wavevector-dependent conductivity $\sigma(\omega, q)$, which was calculated within the random phase approximation in [32], [33], and [38].

III. PATTERNED GRAPHENE STRUCTURES

To optically excite plasmon modes with light coming from air one needs to break translation invariance of the system. This is so because free photons in air are limited to exist only above the light line ($q < \omega/c$), while plasmon modes are found in a deep subwalength regime ($q \gg \omega/c$). One way to do this is to cut a thin ribbon out of a graphene plane. Now, if the width of the ribbon is w, then plasmon will form a standing wave across the ribbon with a resonance condition given by the approximate relation [76] $w \approx m\lambda_p/2$, where m is integer and $\lambda_p = 2\pi/q$ is the wavelength of plasmon from infinite graphene sheet given by (8). This means that we will have a strong absorption of light at the resonance frequency that scales as $\omega_p \propto n_s^{-1/4} \cdot w^{-1/2}$. This was indeed demonstrated experimentally [22] for the case of a periodic assembly of graphene ribbons, which are illustrated in Fig. 3(a). When the microribbon arrays are gated, their optical response changes, and in Fig. 3(b) and (c), we show the change in the transmission spectrum with respect to the charge neutrality point for the electric field parallel and perpendicular to the ribbons, respectively. When the field is parallel to the ribbons, the response is equivalent to a gated graphene plane, i.e., the response can be described by the Drude model [22]. For the perpendicular field, the translation symmetry is broken and a clear evidence of plasmonic resonances appears [Fig. 3(c)] [22]. Plasmon absorption is remarkably strong (more than an order of magnitude larger than that achieved in two-dimensional electron gas in conventional semiconductors) [22].

Note that the absorption cross section is significantly enhanced by using assembly of closely spaced ribbons, compared to the single ribbon, while it was also shown [76] that the interaction between the neighboring ribbons is relatively weak. In fact, only the lowest mode ($m = 1$) will be slightly perturbed [76] when the width of the gap between ribbons is $0.25w$. Nikitin *et al.* [76] also pointed out that, in principle, it should be possible to observe absorption at higher harmonics ($m > 1$), however, the system would need to have extremely low losses, i.e., long scattering time $\tau \approx 10^{-11}$ s (see Section V on losses).

The width of the ribbons discussed above was on the order of micrometers. Plasmons were also theoretically analyzed for the extreme case of few-nanometer-wide graphene ribbons [78], [79], and ribbon arrays [80]. In that case, electronic wavefunctions get quantized across the ribbon, and electronic states dissolve into set of subbands, which in turn changes the plasmon dispersion. Also depending on the exact structure of the edges, ribbons can also acquire a bandgap with typical measured [81] values on the order of ≈200 meV (20 meV) for ribbon widths ≈15 nm (25 nm). Importance of nonlocal and quantum finite size effects was further studied from first principle calculations of the optical response of doped nanostructured graphene [82] and using quantum chemistry semiempirical approaches for elongated graphene nanoflakes of finite length [83]. It was demonstrated [82] that plasmon energies are in a good agreement with classical local electromagnetic theory down to ≈10-nm sizes, while finite size effects were shown to produce substantial plasmon broadening compared to the homogenous graphene sheet up to sizes above 20 nm in disks and 10 nm in ribbons.

Plasmons can also propagate along the graphene nanoribbon in the form of waveguide modes or strongly localized edge modes [77], while the latter ones do not experience a cutoff in frequency and can surpass diffraction limit even in the thin ribbons. Moreover, plasmons

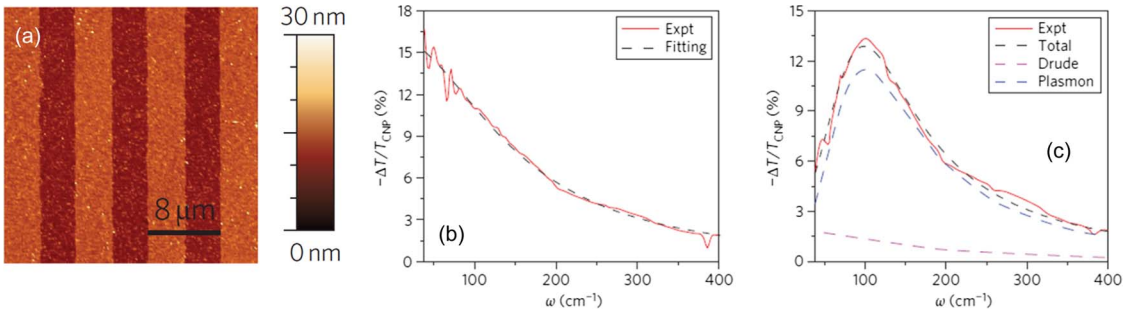

Fig. 3. ***Plasmon resonances in microribbon arrays. (a) Atomic force microscope (AFM) image of a graphene microribbon array sample from [22] with a ribbon width of 4 μm; the width of the ribbon is equal to the separation distance. (b)–(c) Change in the transmission spectra $-\Delta T/T_{CNP}$ induced by gating for the electric field (b) parallel and (c) perpendicular to the ribbons; $\Delta T = T - T_{CNP}$, where T is the transmission of the gated array, and T_{CNP} is the transmission at the charge neutrality point. For perpendicular polarization in (c), the spectrum shows an absorption peak at 3 THz due to plasmon excitation. For parallel polarization, the absorption is described by Drude model. See text and [22] for details (the figures are adapted by permission from Macmillan Publishers Ltd. [22], copyright 2011).***

were also studied under a realistic condition of inhomogeneous electrostatic doping [66], and it was shown that an additional degree of freedom can be obtained by coupling of plasmon modes between two neighboring ribbons [61].

A particularly interesting patterned structure is a periodic assembly of disks in graphene/insulator stacks with several graphene sheets separated by a thin insulating layers [26]; see Fig. 4(a). In samples from [26], there is a strong interaction between the disks sitting on top of each other in different layers while the interaction within a single layer is small or negligible depending on the distance between the disks. The interaction between the layers leads to significant change in both resonance frequency and amplitude, thus enabling a few graphene-plasmon-based devices [26]. By tailoring the size of the disks d, their separation a, and chemical doping, the IBM team created a tunable far-IR notch filter with 8.2-dB rejection ratio, and a tunable THz linear polarizer with 9.5-dB extinction ratio [26]. Fig. 4(b) shows the extinction ratio $1 - T/T_0$ for a single-layer graphene array with $d = 4.4$ μm and two values of separation between the disks, $a = 9$ μm and 4.8 μm. Here, T and T_0 are the transmission through the sample with and without graphene stacked layers present, respectively. The more densely packed array exhibits a higher peak extinction. Fig. 4(c) shows the extinction for different values of d (a is only 400 nm larger than d); in such a densely packed array, peak extinction is as high as 85% corresponding to a notch filter. A linear THz polarizer can be made by using a pattern of microribbon stacks [see the inset in Fig. 4(d)] [26]. The ribbon width is 2 μm and their separation is 0.5 μm (the plasmonic resonance occurs only for electric field perpendicular to the ribbon axis). Fig. 4(d) shows extinction for 0° and 90° polarization (inset shows extinction at 40 cm^{-1} as a function of light polarization). It was also demonstrated [26] that simple unpatterned structure of several graphene layers can serve as an excellent shield of EM radiation for frequencies below 1 THz simply due to Drude response, which increases proportional to the number of layers. Other experiments were performed in microstructures, which offer additional resonances due to hybridization of disk and antidot mode [27].

Terahertz plasmons in micrometer-sized graphene disks (and graphene disk structures) can be tuned by using a magnetic field (perpendicular to the graphene disks) [29]. It has been argued that plasmon resonance in graphene disks splits into edge and bulk plasmon modes under the influence of a strong magnetic field. The distance (in the frequency domain) between the two resonances increases with increasing field. The splitting rate depends on doping. Interestingly, the lifetime of the edge plasmon mode also *increases* with the increase of the field. These experiments point out that graphene might be used in tunable THz magneto–optical devices [29].

The applicability of periodically patterned graphene structures is underpinned by recent theoretical papers [47], [65], predicting large extinction cross sections of graphene disks, which can exceed their geometrical area by an order of magnitude. Additionally, it was shown that arrays of doped graphene disks could allow total optical absorption when supported on a substrate, under total internal reflection or when lying on a dielectric layer coating a metal [65].

Graphene has also been considered in the context of optical antennas, which can convert far-field radiation into localized energy and *vice versa*. They are conventionally built from metals, and they are based on point-metallic plasmons. Tunable terahertz optical antennas with graphene ring structures were proposed [60]. Plasmonic resonances of the concentric and experimentally relevant nonconcentric graphene rings can be tuned not only by changing the size of the rings (as metallic antennas), but also by changing the doping concentrations. By increasing the Fermi energy, it was shown that resonances of

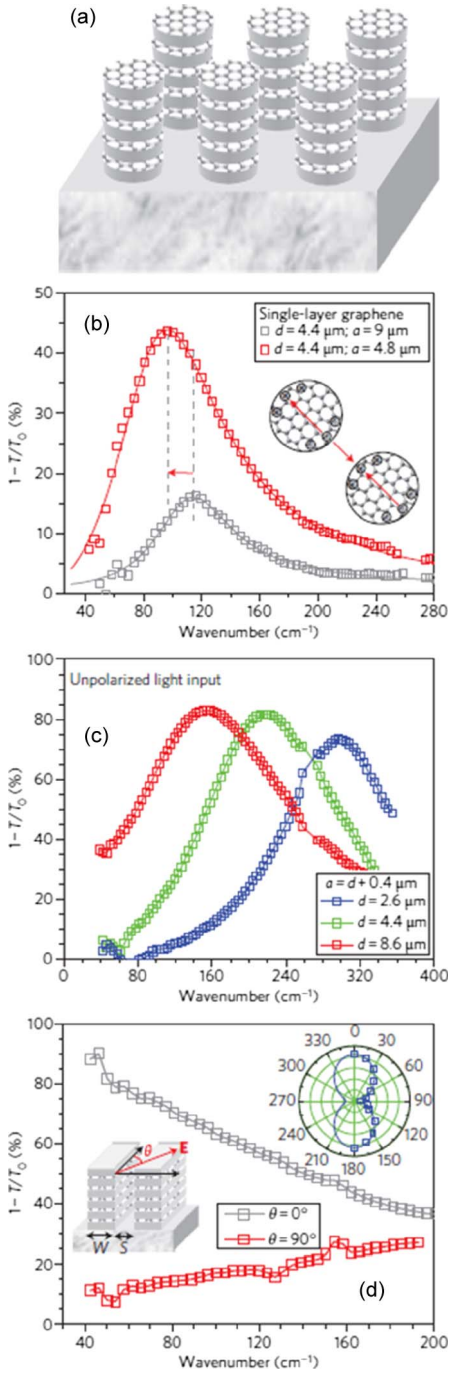

Fig. 4. ***Plasmon resonances in microdisk arrays. (a) Schematic illustration of the patterned graphene/insulator stacks. (b) Extinction spectra $1 - T/T_0$ in single-layer graphene plasmonic devices for different separation between the disks. Inset illustrates the graphene disk–disk interaction. (c) Extinction in transmission of tunable THz filters, which can be tuned by varying the diameter of the disks; stacked devices with five graphene layers were used. (d) Extinction spectra of a graphene THz polarizer made of microribbons (left inset) for polarizations along ($\theta = 0^\circ$) and perpendicular ($\theta = 90^\circ$) to the micro-ribbons. Right inset shows a polar plot of extinction versus polarization at 40 cm^{-1}. See text and [26] for details (the figures are adapted by permission from Macmillan Publishers Ltd. [26], copyright 2012).***

concentric rings are blue shifted, and the extinction cross sections are increased. As an advantage over metallic antennas, the resonance frequencies of graphene antennas mostly lie in the IR and THz ranges, which is important because biological materials have molecular vibration frequencies in those frequency regions [60].

Instead of mechanically cutting graphene into ribbons, plasmons can also be confined into various waveguide structures [58], [62] by tailoring the space dependence of electron concentration, i.e., conductivity in graphene. This can be performed through electrostatic doping, for example, by changing the thickness or permittivity of dielectric spacer lying between a graphene and the electric gate. As such, graphene provides an exciting platform for metamaterials and transformation optical devices [58]. In that regards, it was predicted [59] that a single sheet of graphene with properly designed, nonuniform conductivity distribution can act as a convex lens for propagating plasmon waves, which may yield spatial Fourier transform of IR SPP signals.

It was also predicted [84] and experimentally demonstrated [30] that atomic impurities can localize plasmon modes in graphene on subnanometer scales. However, these measurements [30] deal with petahertz ($\approx$10 eV) frequency regime, which means they involve π ($\approx$4.5 eV) and $\pi + \sigma$ ($\approx$15 eV) plasmons [85], which are located in the continuum of electron–hole excitations and are, therefore, very severely damped. At these energies, it is also necessary to go beyond the linear Dirac cone approximation and consider the full band structure of graphene.

IV. NANOIMAGING AND NANOSCOPY OF PLASMONS IN GRAPHENE

Several recent exciting experiments have imaged graphene plasmons in real space and performed nanoscopy measurements by using the so-called scattering-type near-field microscopy (s-SNOM) [23]–[25]. The basic idea is to illuminate a sharp tip of an atomic force microscope (the tip size is $a \approx 25$ nm) with infrared light; the tip in turn acts like a nanodipole emitter which spans momenta extending up to a few times of $1/a$ at IR frequency. This enables matching of both the frequency and wavevector to excite graphene plasmons. The tip is located at some distance d above the graphene overlaid on a dielectric substrate (e.g., SiO_2), but also in the vicinity of the edge of a graphene sample [24], or above a nanoribbon [25]. This experimental setup is illustrated in Fig. 5(a) [24], [25]. Plasmons that are excited by dipole oscillations from the illuminated tip reflect from the sample edges and form standing waves. The observable of the method is a measure of the electric field inside the gap between the tip and the sample. Since this field is directly related to the plasmon amplitude by measuring the field at different positions above, the sample one effectively measures the field of plasmon standing waves.

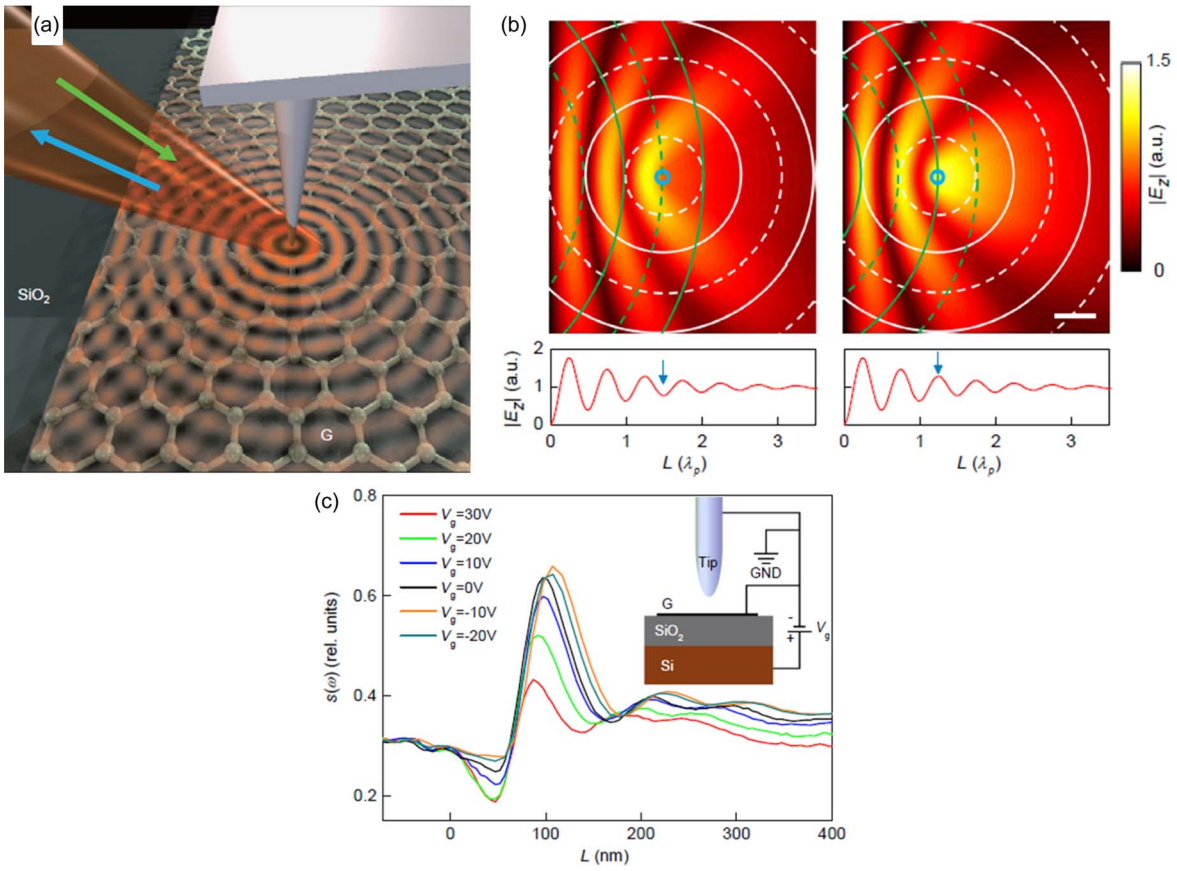

Fig. 5. ***(a) Schematic illustration of the infrared nanoimaging experiments. (b) Interference structure of a plasmon launched from the tip and reflected plasmon waves from the edge of the sample; left and right panels show constructive and destructive interference underneath the tip. Solid (dashed) lines correspond to the positive (negative) field maxima. Graphene is in the $L > 0$ region. (c) The signal (observable) for different gate voltages. See text and [24] for details (the figures are adapted by permission from Macmillan Publishers Ltd. [24], copyright 2012).***

Fig. 5(b) illustrates the amplitude of the electric field formed between the tip and the edge; solid and dashed lines point at the field maxima and minima, respectively. In Fig. 5(c), we illustrate measurements of the observable for different gate voltages, which clearly show that graphene plasmons can be tuned via gate voltage. The analysis of measurements shows that plasmon wavelength approximately follows the law $\lambda_p \propto \sqrt{|n|^2}$, where n is the carrier (hole in this case) density; λ_p is obtained from (complex) plasmon wavevector $q_p = q_1 + iq_2$ via $\lambda_p = 2\pi/q_1$. Measurements show very strong confinement of the EM energy, that is, $\lambda_{\text{air}}/\lambda_p \approx 55$ at $\lambda_{\text{air}} = 11.2\ \mu$m; despite of such strong confinement, plasmons can propagate several times λ_p. However, measurements of [24] did not show change of the plasmon damping rate $q_2/q_1 \approx 0.135 \pm 0.015$ with the gate voltage, which is expected in the independent electron picture, so it would be interesting to address this issue in future experiments. The sample mobility from [24] was $\mu \approx 8000$ cm^2/Vs. The question of which processes are responsible for plasmon damping is still open, and we will address it in subsequent sections.

We point out that the nanoimaging method outlined above was successfully used to measure real-space images of plasmons in graphene nanoribbons on different substrates [25]. Coupling of plasmons with surface optical phonons of the substrate was observed with nanoscopy measurements in this setup [23]. Efficient excitation of graphene plasmons and strong-light matter interaction corresponding to the nanoimaging setup was analyzed in [46]–[48].

V. MANY-BODY EFFECTS AND PLASMONIC LOSSES

Solid state systems involve complex interactions of various elementary excitations (electrons, phonons, excitons, etc.) that can lead to exotic states of matter like in the case of superconductivity [86] and fractional quantum Hall effect [87], [88]. These phenomena fall under the

general domain of many-body physics, and graphene provides an exciting platform for their exploration. In that context, graphene can support plasmons which are basically density oscillations involving collective coherent excitation of the interacting electron gas. It was shown that this plasmon mode can interact with other elementary excitations like a single electron to form a composite particle plasmaron [89] or with a phonon mode (substrate phonons or intrinsic graphene phonons) to form a hybrid plasmon–phonon mode [39], [40]. On the other hand, this interaction can also lead to plasmon decay through excitation of an electron–hole pair or electron–hole pair and a phonon.

The question of plasmonic losses is particularly intriguing and important. The search for low-loss plasmonic materials is still underway [3] due to the great potential that plasmons have for the development of nanophotonics. As we have already mentioned, plasmon dispersion is usually calculated within the RPA method, which captures the possibility of plasmon decay via emission of electron–hole pairs. These strong interband losses occur only above some threshold frequency in the (ω, q) space [see Fig. 2(b)], since Pauli principle does not allow excitation of electrons into the state that is already occupied. The threshold frequency depends on doping, and by increasing the gate voltage, these strong interband losses can be eliminated for frequencies in the THz and IR (e.g., see [38]).

However, even below this threshold, other processes can lead to plasmon damping. These processes can be introduced phenomenologically into the theoretical calculation by employing the relaxation-time approximation into the RPA procedure [38], where relaxation time τ contains information on the plasmon decay via all admissible channels. If we assume independent decay channels, we can write τ as

$$\frac{1}{\tau(\omega)} = \frac{1}{\tau_{\text{imp}}(\omega)} + \frac{1}{\tau_{\text{Aph}}(\omega)} + \frac{1}{\tau_{\text{Oph}}(\omega)} + \frac{1}{\tau_{e-e}(\omega)} \quad (11)$$

where τ_{imp} denotes the contribution to the plasmon damping from scattering on impurities and defects, τ_{Aph} from acoustic phonons, τ_{Oph} from optical phonons, and τ_{e-e} from electron–electron interactions beyond RPA; generally τ can depend strongly on frequency ω.

As a starting point for estimating the relaxation time values, one may choose to use direct current (dc) measurements. In graphene, the dc measurements are most usually expressed through mobility which is given by $\mu = \sigma(\omega = 0)/n_s e$, where n_s is the surface density of electrons. By using the Drude model for graphene from (7), we can write the relaxation time as $\tau_{\text{dc}} = \mu\hbar\sqrt{n_s\pi}/ev_F$, which depends on the electron density n_s. Typical measured [10] room-temperature mobilities are $\mu = 10\ 000\ \text{cm}^2/\text{Vs}$ at densities $n_s = 10^{13}\ \text{cm}^{-2}$, which gives very long relaxation time $\tau_{\text{dc}} = 370$ fs. These values are most likely dictated by Coulomb scattering of the charged impurities residing on graphene or in the underlying substrate [95]. Indeed, it was demonstrated [96] that room-temperature mobilities can reach $\approx 60\ 000\ \text{cm}^2/\text{Vs}$ for graphene suspended in liquid of high dielectric constant, which screens Coulomb interactions with impurities. This experiment was performed under significantly lower doping $n_s = 5 \times 10^{11}\ \text{cm}^{-2}$, which gives relaxation time $\tau_{\text{dc}} \approx 500$ fs. Finally, we note that graphene suspended in air, which was annealed to remove impurities, shows [97] only a modest increase of the resistivity from 5 to 240 K, maintaining a mobility of $\mu = 120\ 000\ \text{cm}^2/\text{Vs}$ at 240 K and density $n_s = 2 \times 10^{11}\ \text{cm}^{-2}$, which corresponds to $\tau_{\text{dc}} \approx 630$ fs. In Fig. 6(a), we illustrate the losses $(\Re q/\Im q)$ of graphene's plasmons as a function of frequency; the solid line corresponds to losses estimated from $\tau_{\text{dc}} = 640$ fs.

By measuring the plasmon linewidths, recent experiments [26], [27], [29] have demonstrated that dc relaxation time of $\tau \approx 100$ fs does not significantly change for plasmons of several THz frequency. However, several different experimental techniques [18], [19], [24], [90] have demonstrated reduction of relaxation time at higher (mid- and near-IR) frequencies compared to the dc relaxation times.

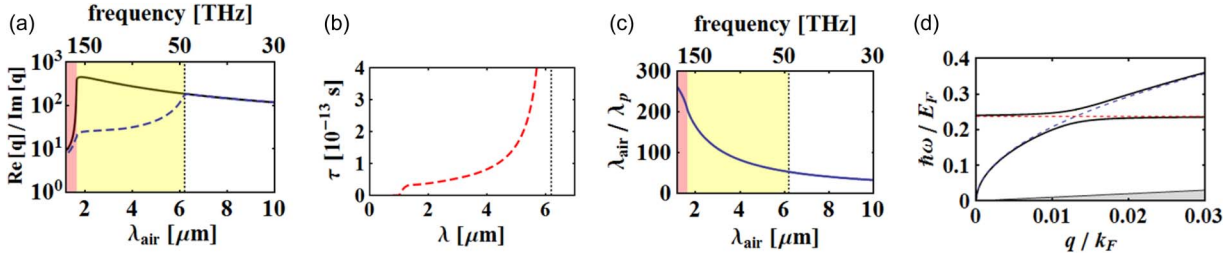

Fig. 6. *Plasmon properties including losses, relaxation times, and dispersion of the plasmon–phonon coupled modes. (a) Plasmon losses quantified as $\Re q/\Im q$ calculated by using only dc relaxation time $\tau_{\text{dc}} = 640$ fs (solid line) and $\tau_{\text{dc}} = 640$ fs as well as $\tau_{\text{Oph}}(\omega)$ (dashed line), which is displayed in (b). The leftmost shaded region (rose) depicts the region of interband losses. The central region shaded in yellow depicts the region where losses from optical phonons are important. (c) Localization of graphene plasmons quantified as $\lambda_{\text{air}}/\lambda_p$. The parameters for (a), (b), and (c) are $n_s = 3 \times 10^{13}\ \text{cm}^{-2}$, $\mu = 10\ 000\ \text{cm}^2/\text{Vs}$, substrate is SiO_2. (d) Plasmon–phonon dispersion curve for doping $n_s = 5 \times 10^{13}\ \text{cm}^{-2}$. See text for details.*

This was seen in optical absorption experiment on uniform graphene [18] but also on graphene nanoribbons [90]. Note, however, that graphene ribbons in the experiment [90] are around 100 nm in width so that edge scattering can severely limit the dc relaxation time. A view of the experiment [90] can be found in [91]. On the other hand, another experiment [92] on graphene nanorings of similar size (100 nm) has observed different behavior of increase of relaxation time in the near-IR compared to the dc relaxation time.

A very different experimental technique (EELS) has demonstrated [19] that plasmon linewidth increases linearly with plasmon momentum, which amounts to a decrease of relaxation time with frequency. Finally, the IR nanoscopy experiment [24] has demonstrated decrease of relaxation time from a dc value $\tau_{\rm dc} = 260$ fs to a lower value $\tau = 75$ fs at 27-THz frequency. These measurements [24] were performed on graphene samples with $n_s = 8 \times 10^{12}$ cm^{-2} doping, $\mu = 8000$ cm^2/Vs mobilities, and the measured plasmon wavelength was on the order of 200 nm, which was around 55 times smaller than the corresponding wavelength (11 μm) of light at the frequency of 27 THz. Plasmon wavelength and propagation distance were measured in real space obtaining $\Re q/\Im q = 7.4$. These measurements were performed on a lossy substrate. Nevertheless, by extrapolating these numbers to a lossless substrate, one would obtain $\Re q/\Im q = 12.7$.

Let us now discuss the influence of phonons on the optical relaxation time by using silver (which has well-know properties) as an example. The optical properties of silver are easily fitted to the Drude response given by (5) with the relaxation time [93] of the order $\tau_{\rm opt} \approx 30$ fs. Note that this is of the same order of magnitude as the relaxation time obtained [68] from the dc measurements of conductivity $\sigma(\omega = 0)$ at room temperature: $\tau_{\rm dc}(T = 273\ {\rm K}) = 40$ fs. One would thus be led to believe that dc measurements are sufficient to estimate the optical relaxation time. However, note that at lower temperatures one obtains significantly longer dc relaxation times [68] $\tau_{\rm dc}$ ($T = 77$ K) $= 200$ fs, which signals large influence of phonon scattering. Holstein [94] gave a simple explanation of this behavior by noting that low-temperature optical relaxation time is related to the high-temperature dc relaxation time. To understand this, note that in dc measurements electron energy available for generation of an individual phonon is roughly kT, so only a small number of phonon modes are excited in the case $T \ll \Theta_D$, where $\Theta_D = 215$ K is Debye temperature in silver [68]. However, at optical frequencies, when $\hbar\omega \gg k\Theta_D$, all the phonon modes can be excited, which looks more like the case of high-temperature dc measurements. On the other hand, for $T \gg \Theta_D$, there will also be a significant contribution to dc conductivity from the phonon absorption, which is not present at low-temperature optical measurements. However, this is easily accounted for by noting that the ratio of phonon absorption and emission is proportional to the number of thermally excited phonon modes, which is roughly $n = (1/e^{\Theta_D/T} - 1) \approx (T/\Theta_D)$, when $T \gg \Theta_D$. Finally, Holstein gives estimate of the optical relaxation time

$$\tau_{\rm opt} \approx \tau_{\rm dc}(T)\frac{T}{\Theta_D} \tag{12}$$

where T is some reference temperature larger than the Debye temperature Θ_D.

By returning to the case of graphene, let us first note that the measured long dc relaxation times and weak temperature dependence signify weak phonon scattering, which is indeed expected in graphene due to the very high Debye temperature $\Theta_D \approx 2000$ K. However, the Holstein argument [94] then states that contribution to the optical relaxation time can hardly be deduced from the room-temperature dc measurements in graphene. In addition to that, besides acoustical phonons (which are limited by Debye temperature), graphene also supports optical phonons on the same order of magnitude as Debye temperature $\hbar\omega_{\rm Oph} \approx 0.2$ eV. We have argued [38] that, due to the strong electron–phonon interaction with these optical phonon modes, optical relaxation time $\tau_{\rm Oph}(\omega)$ for frequencies above $\omega_{\rm Oph}$ drops down to tens of femtoseconds [see Fig. 6(b)]. Plasmon losses corresponding to $\tau_{\rm Oph}(\omega)$ are shown in Fig. 6(a) (dashed line); localization parameter $\lambda_{\rm air}/\lambda_p$ does not depend on τ; see Fig. 6(c). In this process, a photon (i.e., a plasmon) is allowed to excite electron–hole pair even below the interband threshold, by emitting one optical phonon mode, which provides the necessary momentum. On the other hand, phonon absorption is insignificant unless we are working at very high temperatures. Since an optical phonon needs to be created, the photon (plasmon) needs to have energy $\hbar\omega \geq \hbar\omega_{\rm Oph}$, due to energy conservation. In other words, for frequencies (wavelengths) below $f_{\rm Oph} \approx 50$ THz (above $\lambda_{\rm Oph} \approx 6$ μm, respectively) these losses are kinematically forbidden, and we expect a sharp decrease of the relaxation time above the optical phonon frequency. It can be expected that by considering also acoustical phonons, this transition will be more gradual with the relaxation time steadily decreasing, as we approach Debye frequency $\omega_D = k\Theta_D/\hbar$. On the other hand, room-temperature dc measurements will show significantly longer relaxation times since most of these phonon modes will be effectively frozen due to their high excitation energies.

The contribution from electron–electron correlations beyond RPA to the optical conductivity was theoretically calculated in [98] and [99]. It was pointed out that these processes would induce severe plasmon losses below the interband threshold [100]. Nevertheless, additional theoretical and experimental research is required to fully understand the contribution from phonons and electron–electron correlations to plasmon losses.

Plasmons can also strongly interact with surface phonon modes of the polar substrate to form a hybrid plasmon–phonon mode [39], which was experimentally demonstrated with several different techniques [20], [23], [25], [27]. This can be understood as a simple first-order process when plasmon and phonon dispersions cross, so that the electron–phonon interaction gets significantly enhanced through the collective electron response described by the zero of the dielectric function. We would like to emphasize that there is also an intriguing hybridization of the plasmon with the intrinsic optical phonon in graphene [40], which is illustrated in Fig. 6(d). Away from the crossing point, the excitations have a clear plasmonic and phononic character, whereas in the vicinity of the crossing, the hybridization is strong. As an interesting consequence of the unique electron–phonon interaction in graphene, we mention unconventional mixing of plasmon and optical phonon polarizations: Longitudinal plasmons in graphene couple exclusively to transverse optical phonons, whereas graphene's transverse plasmons couple only to longitudinal optical phonons [40].

VI. PLASMONS IN METALLIC MONO-ATOMIC LAYERS

Plasmons were also demonstrated in ultrathin metallic layers and monolayers [7]–[9], which have an advantage over graphene: they have an abundance of free carriers even in intrinsic, i.e., undoped, case. For example, for monovalent metals like silver, the surface density of electrons is around $n_s \approx n_v^{2/3}$ for a monolayer crystal. Here, $n_v = 5.9 \times 10^{22}$ cm^{-3} is the volume density of electrons in bulk silver [68], so $n_s = 1.5 \times 10^{15}$ cm^{-2}, which is very difficult to obtain in graphene.

Next, we need to consider intraband and interband transitions which can induce strong plasmon damping. It is straightforward to demonstrate that the onset of intraband transitions for the case of silver on silicon is rather high (around 4-eV energy). This is actually comparable to the threshold for interband transitions [93] from lower d band in bulk silver so we can take it as an estimate for the cutoff frequency (4 eV corresponds to 300-nm wavelength). This is another advantage of metallic monolayers compared to the graphene case, since such a high cutoff frequency could be obtained only in a very doped graphene. By using a simple Drude model to describe plasmon dispersion given by (6), we obtain plasmon wavelengths two orders of magnitude lower than the corresponding free-space wavelength of light [see Fig. 7(a)]. We can also estimate losses by using relaxation time from the bulk silver case $\tau \approx 30$ fs, which is shown in Fig. 7(b). Note that relaxation time of a metallic monolayer can be different from the case of bulk material, or can, in general, have some frequency dependence. In fact, the EELS experiment on silver monolayer demonstrated [7] huge plasmon linewidth that increases linearly with plasmon momentum, similar to the case of graphene

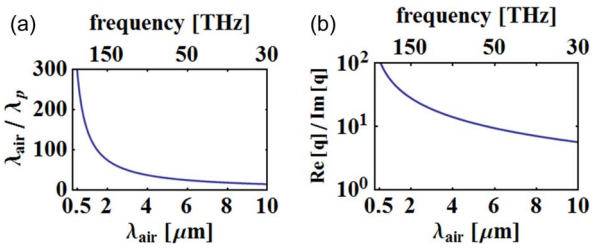

Fig. 7. *Properties of plasmons in metallic monolayers. (a) Ratio of free-space wavelength to the plasmon wavelength in the case of plasmon in a monoatomic layer of silver. (b) Plasmon propagation length in unit of plasmon wavelength.*

[19]. Note, however, that domain sizes of these metallic monolayer, reported in [7], are only of the order of 100 nm.

One tremendously important advantage of graphene over metallic monolayer is its mechanical stability. While metallic monolayers were only demonstrated to exist on a substrate, graphene can maintain its structural integrity even in a suspended form.

VII. DISCUSSION, CONCLUSION, AND OUTLOOK

Before concluding, let us outline several other interesting directions of research related to graphene plasmons. It was predicted that thermally excited plasmons can strongly mediate, enhance, and tune the near-field radiation transfer between two closely separated graphene sheets [101]. The resultant heat transfer can be several orders of magnitude greater than the far-field heat transfer between two black bodies of the same temperatures limited by the Stefan–Boltzman law. The reason for this is easily understood by noting that plasmon dispersion in graphene is in deep subwavelength regime ($q \gg \omega/c$) with large density of plasmon states. Then, since each wavevector can be considered as a separate heat channel, these plasmon modes can transfer significantly larger amount of heat than the free propagating modes, which are limited by the light line ($q < \omega/c$). Of course, due to the evanescent nature of the fields, graphene sheets have to be very close (on the order of a micrometer) for this effect to take place. It was further predicted that graphene can be used as a hot emitter in the near-field thermo–photovoltaic systems, resulting in high-power densities and device efficiencies [102].

Plasmons get damped during propagation, as we discussed in Section V. However, if graphene is illuminated by a pump light source, its conductivity will change and can become negative [36], [63], [64]. This happens because electrons under illumination create population inversion. Under such nonequilibrium conditions, plasmon can get amplified during propagation [36], [64] via stimulated

emission of plasmons. Coherent terahertz sources based on such amplification were suggested [36], [63].

Graphene plasmons are attracting interest in the context of magneto–optics [28]. When a magnetic field perpendicular to the graphene sheet is applied, cyclotron excitations and plasmons interact and can hybridize to form the so-called magnetoplasmon modes [51]–[53], which, in turn, dramatically changes the magneto–optical response, such as the Faraday rotation. This occurs because the cyclotron mass in graphene is two orders of magnitude smaller than in conventional metallic plasmonic materials, which promotes graphene as a unique material for investigating magneto–optical phenomena. As an example, we point at experiments performed in [28], where the magnetic field perpendicular to a graphene sheet overlaid on a SiC substrate was applied, and electromagnetic radiation perpendicular to the graphene sheet was applied. As a consequence, the existence of terraces (and wrinkles) in the sample, translational invariance is broken, and magnetoplasmons are excited. Interestingly, the plasmonic resonance splits into two peaks with increasing magnetic field, in striking resemblance with the splitting observed in graphene disks patterned structures with the magnetic field applied [29]. The direction of the linearly polarized light is rotated after passing through the sample, which is a clear demonstration of Faraday rotation [28].

It is interesting to note then when strain is applied on graphene, i.e., when it is somehow stretched or bent, electron dynamics can be accounted for by adding an effective vector gauge potential to the Dirac equations governing the dynamics in nonstretched graphene. This can effectively be interpreted as an effective magnetic field applied to the sample which can exceed in value the field values obtained with the real magnetic field. Strain will thus also affect plasmons, which has been addressed in a few studies [54], [55].

After reviewing the rapidly growing literature related to plasmons and plasmonic effects in graphene and graphene-based structures, we conclude that graphene plasmonics is a very promising area of research, both from the point of view of fundamental physics and exploring novel physical effects, but also with a great potential for applications. Graphene plasmons have several potential advantages over surface-plasmon polaritons on metal–insulator surfaces. First, their properties can be tuned, either by applying the gate voltage or chemical doping. The plasmonic resonances are also tunable, and they can range from THz frequencies up to optical frequencies depending on the doping. Second, plasmonic losses via excitation of electron–hole pairs can also be eliminated via doping, such that plasmons are damped via second-order processes. The electromagnetic energy confinement is very strong for graphene plasmons. Experiments have achieved the ratio of the plasmon wavelength to the wavelength of light in air (at the same frequency) on the order of $\lambda_{air}/\lambda_p \sim 50$, with simultaneous propagation length of several wavelengths; the propagation length is expected to be even larger when better substrates and cleaner samples are used. Confinement and control of electromagnetic energy below subwavelength scales is important for shrinking optical devices and their integration with electronics. Moreover, it enables great nonlinear enhancements and nonlinear effects. A particularly interesting and promising research direction focuses on patterned structures such as graphene nanoribbon structures and disks; due to a lack of translational symmetry, plasmons are easily excited in those structures, even with freely propagating photons, thus yielding very promising and tunable optical properties, as discussed above. ■

REFERENCES

[1] W. L. Barnes, A. Dereux, and T. W. Ebbesen, "Surface plasmon subwavelength optics," *Nature*, vol. 424, pp. 824–830, 2003.

[2] S. A. Maier and H. A. Atwater, "Plasmonics: Localization and guiding of electromagnetic energy in metal/dielectric structures," *J. Appl. Phys.*, vol. 98, 2005, 011101.

[3] P. R. West, S. Ishii, G. V. Naik, N. K. Emani, V. M. Shalaev, and A. Boltasseva, "Searching for better plasmonic materials," *Laser Photon. Rev.*, vol. 4, pp. 795–808, 2010.

[4] A. Karalis, E. Lidorikis, M. Ibanescu, J. D. Joannopoulos, and M. Soljačić, "Surface-plasmon-assisted guiding of broadband slow and subwavelength light in air," *Phys. Rev. Lett.*, vol. 95, 2005, 063901.

[5] S. J. Allen, D. C. Tsui, and R. A. Logan, "Observation of 2-dimensional plasmon in silicon inversion layers," *Phys. Rev. Lett.*, vol. 38, pp. 980–983, 1977.

[6] E. Batke, D. Heitmann, and C. W. Tu, "Plasmon and magnetoplasmon excitation in two-dimensional electron space charge layers on GaAs," *Phys. Rev. B*, vol. 34, pp. 6951–6960, 1986.

[7] T. Nagao, T. Hildebrandt, M. Henzler, and S. Hasegawa, "Dispersion and damping of a two-dimensional plasmon in a metallic surface-state band," *Phys. Rev. Lett.*, vol. 86, pp. 5747–5750, 2001.

[8] Y. Yu, Y. Jiang, Z. Tang, Q. Guo, J. Jia, Q. Xue, K. Wu, and E. Wang, "Thickness dependence of surface plasmon damping and dispersion in ultrathin Ag films," *Phys. Rev. B*, vol. 72, 2005, 205405.

[9] Z. Yuan, Y. Jiang, Y. Gao, M. Kall, and S. Gao, "Symmetry-dependent screening of surface plasmons in ultrathin supported films: The case of Al/Si(111)," *Phys. Rev. B*, vol. 83, 2011, 165452.

[10] K. S. Novoselov, A. K. Geim, S. V. Morozov, D. Jiang, Y. Zhang, S. V. Dubonos, I. V. Grigorieva, and A. A. Firsov, "Electric field effect in atomically thin carbon films," *Science*, vol. 306, pp. 666–669, 2004.

[11] K. S. Novoselov, D. Jiang, F. Schedin, T. J. Booth, V. V. Khotkevich, S. V. Morozov, and A. K. Geim, "Two-dimensional atomic crystals," *Proc. Nat. Acad. Sci. USA*, vol. 102, 2005, 10451.

[12] K. S. Novoselov, A. K. Geim, S. V. Morozov, D. Jiang, M. I. Katsnelson, I. V. Grigorieva, S. V. Dubonos, and A. A. Firsov, "Two dimensional gas of massless Dirac fermions in graphene," *Nature*, vol. 438, pp. 197–200, 2005.

[13] Y. Zhang, Y. W. Tan, H. L. Stormer, and P. Kim, "Experimental observation of the quantum Hall effect and Berry's phase in graphene," *Nature*, vol. 438, pp. 201–204, 2005.

[14] A. K. Geim and K. S. Novoselov, "The rise of graphene," *Nature Mater.*, vol. 6, pp. 183–191, 2007.

[15] C. Berger, Z. Song, T. Li, X. Li, A. Y. Ogbazghi, R. Feng, Z. Dai, A. N. Marchenkov, E. H. Conrad, P. N. First, and W. A. de Heer, "Ultrathin epitaxial graphite: 2D electron gas properties and route towards graphene-based nanoelectronics," *J. Phys. Chem. B*, vol. 108, 2004, 19912.

[16] C. Berger, Z. Song, X. Li, X. Wu, N. Brown, C. Naud, D. Mayou, T. Li,

J. Hass, A. N. Marchenkov, E. H. Conrad, P. N. First, and W. A. de Heer, "Electronic confinement and coherence in patterned epitaxial graphene," *Science*, vol. 312, pp. 1191–1196, 2006.

[17] F. Wang, Y. Zhang, C. Tian, C. Girit, A. Zettl, M. Crommie, and Y. R. Shen, "Gate-variable optical transitions in graphene," *Science*, vol. 320, pp. 206–209, 2008.

[18] Z. Q. Li, E. A. Henriksen, Z. Jiang, Z. Hao, M. C. Martin, P. Kim, H. L. Stormer, and D. N. Basov, "Dirac charge dynamics in graphene by infrared spectroscopy," *Nature Phys.*, vol. 4, pp. 532–535, 2008.

[19] Y. Liu, R. F. Willis, K. V. Emtsev, and T. Seyller, "Plasmon dispersion and damping in electrically isolated two-dimensional charge sheets," *Phys. Rev. B*, vol. 78, 2008, 201403(R).

[20] Y. Liu and R. F. Willis, "Plasmon-phonon strongly coupled mode in epitaxial graphene," *Phys. Rev. B*, vol. 81, 2010, 081406(R).

[21] R. J. Koch, T. Seyller, and J. A. Schaefer, "Strong phonon-plasmon coupled modes in the graphene/silicon carbide heterosystem," *Phys. Rev. B*, vol. 82, no. 201413, 2010.

[22] L. Ju, B. Geng, J. Horng, C. Girit, M. Martin, Z. Hao, H. A. Bechtel, X. Liang, A. Zettl, Y. R. Shen, and F. Wang, "Graphene plasmonics for tunable terahertz metamaterials," *Nature Nanotechnol.*, vol. 6, pp. 630–634, 2011.

[23] Z. Fei, G. O. Andreev, W. Bao, L. M. Zhang, A. S. McLeod, C. Wang, M. K. Stewart, Z. Zhao, G. Dominguez, M. Thiemens, M. M. Fogler, M. J. Tauber, A. H. Castro-Neto, C. N. Lau, F. Keilmann, and D. N. Basov, "Infrared nanoscopy of Dirac plasmons at the graphene-SiO_2 interface," *Nano Lett.*, vol. 11, pp. 4701–4705, 2011.

[24] Z. Fei, A. S. Rodin, G. O. Andreev, W. Bao, A. S. McLeod, M. Wagner, L. M. Zhang, Z. Zhao, M. Thiemens, G. Dominguez, M. M. Fogler, A. H. Castro-Neto, C. N. Lau, F. Keilmann, and D. N. Basov, "Gate-tuning of graphene plasmons revealed by infrared nano-imaging," *Nature*, vol. 487, pp. 82–85, 2012.

[25] J. Chen, M. Badioli, P. Alonso-Gonzalez, S. Thongrattanasiri, F. Huth, J. Osmond, M. Spasenović, A. Centeno, A. Pesquera, P. Godignon, A. Zurutuza, N. Camara, J. Garcia de Abajo, R. Hillenbrand, and F. Koppens, "Optical nano-imaging of gate-tuneable graphene plasmons," *Nature*, vol. 487, pp. 77–81, 2012.

[26] H. Yan, X. Li, B. Chandra, G. Tulevski, Y. Wu, M. Freitag, W. Zhu, P. Avouris, and F. Xia, "Tunable infrared plasmonic devices using graphene/insulator stacks," *Nature Nanotechnol.*, vol. 7, pp. 330–334, 2012.

[27] H. Yan, F. Xia, Z. Li, and P. Avouris, "Plasmonics of coupled graphene micro-structures," *New J. Phys.*, vol. 14, 2012, 125001.

[28] I. Crassee, M. Orlita, M. Potemski, A. L. Walter, M. Ostler, T. Seyller, I. Gaponenko, J. Chen, and A. B. Kuzmenko, "Intrinsic terahertz plasmons and magnetoplasmons in large scale monolayer graphene," *Nano Lett.*, vol. 12, pp. 2470–2474, 2012.

[29] H. Yan, Z. Li, X. Li, W. Zhu, P. Avouris, and F. Xia, "Infrared spectroscopy of tunable Dirac terahertz magneto-plasmons in graphene," *Nano Lett.*, vol. 12, pp. 3766–3771, 2012.

[30] W. Zhou, J. Lee, J. Nanda, S. T. Pantelides, S. J. Pennycook, and J.-C. Idrobo, "Atomically localized plasmon enhancement in monolayer graphene," *Nature Nanotechnol.*, vol. 7, pp. 161–165, 2012.

[31] O. Vafek, "Thermoplasma polariton within scaling theory of single-layer graphene," *Phys. Rev. Lett.*, vol. 97, 2006, 266406.

[32] B. Wunsch, T. Sauber, F. Sols, and F. Guinea, "Dynamic polarization of graphene at finite doping," *New J. Phys.*, vol. 8, 2006, 318.

[33] E. H. Hwang and S. Das Sarma, "Dielectric function, screening, plasmons in two-dimensional graphene," *Phys. Rev. B*, vol. 75, 2007, 205418.

[34] V. Ryzhii, A. Satou, and T. Otsuji, "Plasma waves in two-dimensional electron-hole system in gated graphene heterostructures," *J. Appl. Phys.*, vol. 101, 2007, 024509.

[35] S. A. Mikhailov and K. Zeigler, "New electromagnetic mode in graphene," *Phys. Rev. Lett.*, vol. 99, 2007, 016803.

[36] F. Rana, "Graphene terahertz plasmon oscillators," *IEEE Trans. Nanotechnol.*, vol. 7, no. 1, pp. 91–99, Jan. 2008.

[37] S. Gangadharaiah, A. M. Farid, and E. G. Mishcenko, "Charge response function and a novel plasmon mode in graphene," *Phys. Rev. Lett.*, vol. 100, 2008, 166802.

[38] M. Jablan, H. Buljan, and M. Soljačić, "Plasmonics in graphene at infrared frequencies," *Phys. Rev. B*, vol. 80, 2009, 245435.

[39] E. H. Hwang, R. Sensarma, and S. Das Sarma, "Plasmon-phonon coupling in graphene," *Phys. Rev. B*, vol. 82, 2010, 195406.

[40] M. Jablan, M. Soljačić, and H. Buljan, "Unconventional plasmon-phonon coupling in graphene," *Phys. Rev. B*, vol. 83, 2011, 161409.

[41] J. P. Carbotte, J. P. F. LeBlanc, and E. J. Nicol, "Emergence of plasmaronic structure in the near-field optical response of graphene," *Phys. Rev. B*, vol. 85, 2012, 201411(R).

[42] O. Roslyak, G. Gumbs, and D. Huang, "Plasma excitations of dressed Dirac electrons in graphene layers," *J. Appl. Phys.*, vol. 109, 2011, 113721.

[43] S. H. Abedinpour, G. Vignale, A. Principi, M. Polini, W.-K. Tse, and A. H. MacDonald, "Drude weight, plasmon dispersion, ac conductivity in doped graphene sheets," *Phys. Rev B*, vol. 84, 2011, 045429.

[44] C.-H. Park, F. Giustino, C. D. Spataru, M. L. Cohen, and S. G. Louie, "First-principles study of electron linewidths in graphene," *Phys. Rev. Lett.*, vol. 102, 2009, 076803.

[45] F. Rana, J. H. Strait, H. Wang, and C. Manolatou, "Ultrafast carrier recombination and generation rates for plasmon emission and absorption in graphene," *Phys. Rev. B*, vol. 84, 2011, 045437.

[46] A. Yu. Nikitin, F. Guinea, F. J. Garcia-Vidal, and L. Martin-Moreno, "Fields radiated by a nanoemitter in a graphene sheet," *Phys. Rev. B*, vol. 84, 2011, 195446.

[47] F. H. L. Koppens, D. E. Chang, and F. J. García de Abajo, "Graphene plasmonics: A platform for strong light-matter interactions," *Nano Lett.*, vol. 11, pp. 3370–3377, 2011.

[48] K. A. Velizhanin and A. Efimov, "Probing plasmons in graphene by resonance energy transfer," *Phys. Rev. B*, vol. 84, 2011, 085401.

[49] A. R. Davoyan, V. V. Popov, and S. A. Nikitov, "Tailoring terahertz near-field enhancement via two-dimensional plasmons," *Phys. Rev. Lett.*, vol. 108, 2012, 127401.

[50] T. Stauber and G. Gomez-Santos, "Plasmons and near-field amplification in double-layer graphene," *Phys. Rev. B*, vol. 85, 2012, 075410.

[51] R. Roldan, J.-N. Fuchs, and M. O. Goerbig, "Collective modes of doped graphene and a standard two-dimensional electron gas in a strong magnetic field: Linear magnetoplasmons versus magnetoexcitons," *Phys. Rev. B B*, vol. 80, 2009, 085408.

[52] J.-Y. Wu, S.-C. Chen, O. Roslyak, G. Gumbs, and M.-F. Lin, "Plasma excitations in graphene: Their spectral intensity and temperature dependence in magnetic field," *ACS Nano*, vol. 5, pp. 1026–1032, 2011.

[53] A. Ferreira, N. M. R. Peres, and A. H. Castro Neto, "Confined magneto-optical waves in graphene," *Phys. Rev. B*, vol. 85, 2012, 205426.

[54] F. M. D. Pellegrino, G. G. N. Angilella, and R. Pucci, "Dynamical polarization of graphene under strain," *Phys. Rev. B*, vol. 82, 2010, 115434.

[55] F. M. D. Pellegrino, G. G. N. Angilella, and R. Pucci, "Linear response correlation functions in strained graphene," *Phys. Rev. B*, vol. 84, 2011, 195407.

[56] A. Manjavacas, P. Nordlander, and F. J. Garcia de Abajo, "Plasmon blockade in nanostructured graphene," *ACS Nano*, vol. 6, pp. 1724–1731, 2012.

[57] S. A. Mikhailov, "Theory of the giant plasmon-enhanced second-harmonic generation in graphene and semiconductor two-dimensional electron systems," *Phys. Rev. B*, vol. 84, 2011, 045432.

[58] A. Vakil and N. Engheta, "Transformation optics using graphene," *Science*, vol. 332, pp. 1291–1294, 2011.

[59] A. Vakil and N. Engheta, "Fourier optics on graphene," *Phys. Rev. B*, vol. 85, 2012, 075434.

[60] P. Liu, W. Cai, L. Wang, X. Zhang, and J. Xu, "Tunable terahertz optical antennas based on graphene ring structures," *Appl. Phys. Lett.*, vol. 100, 2012, 153111.

[61] J. Christensen, A. Manjavacas, S. Thongrattanasiri, F. H. L. Koppens, and F. J. Garcia de Abajo, "Graphene plasmon waveguiding and hybridization in individual and paired nanoribbons," *ACS Nano*, vol. 6, pp. 431–440, 2012.

[62] E. G. Mishchenko, A. V. Shytov, and P. G. Silvestrov, "Guided plasmons in graphene p-n junctions," *Phys. Rev. Lett.*, vol. 104, 2010, 156806.

[63] V. Ryzhii, M. Ryzhii, and T. Otsuji, "Negative dynamic conductivity of graphene with optical pumping," *J. Appl. Phys.*, vol. 101, 2007, 083114.

[64] A. A. Dubinov, V. Ya. Aleshkin, V. Mitin, T. Otsuji, and V. Ryzhii, "Terahertz surface plasmons in optically pumped graphene structures," *J. Phys., Condens. Matter*, vol. 23, 2011, 145302.

[65] S. Thongrattanasiri, F. H. L. Koppens, and F. J. Garcia de Abajo, "Complete optical absorption in periodically patterned graphene," *Phys. Rev. Lett.*, vol. 108, 2012, 047401.

[66] S. Thongrattanasiri, I. Silveiro, and F. J. Garcia de Abajo, "Plasmons in electrostatically doped graphene," *Appl. Phys. Lett.*, vol. 100, 2012, 201105.

[67] M. Jablan, H. Buljan, and M. Soljačić, "Transverse electric plasmons in bilayer grapheme," *Opt. Exp.*, vol. 19, pp. 11236–11241, 2011.

[68] N. W. Ashcroft and N. D. Mermin, *Solid State Physics*. Philadelphia, PA, USA: Saunders, 1976.

[69] R. R. Nair, P. Blake, A. N. Grigorenko, K. S. Novoselov, T. J. Booth, T. Stauber, N. M. R. Peres, and A. K. Geim, "Fine structure constant defines visual transparency of graphene," *Science*, vol. 320, p. 1308, 2008.

[70] W. H. Backes, F. M. Peeters, F. Brosens, and J. T. Devreese, "Dispersion of longitudinal plasmons for a quasi-two-dimensional electron gas," *Phys. Rev. B*, vol. 45, pp. 8437–8442, 1992.

[71] J. D. Jackson, *Classical Electrodynamics*, 3rd ed. New York, NY, USA: Wiley, 1998.

[72] R. Hillenbrand, T. Taubner, and F. Keilmann, "Phonon-enhanced light-matter interaction at the nanometer scale," *Nature*, vol. 418, pp. 159–162, 2002.

[73] N. Ocelic and R. Hillenbrand, "Subwavelength-scale tailoring of surface phonon polaritons by focused ion-beam implantation," *Nature Mater.*, vol. 3, pp. 606–609, 2004.

[74] P. R. Wallace, "The band theory of graphite," *Phys. Rev.*, vol. 71, pp. 622–634, 1947.

[75] L. A. Falkovsky, "Optical properties of graphene," *J. Phys. Conf. Ser.*, vol. 129, 2008, 012004.

[76] A.Yu. Nikitin, F. Guinea, F. J. Garcia-Vidal, and L. Martin-Moreno, "Surface plasmon enhanced absorption and suppressed transmission in periodic arrays of graphene ribbons," *Phys. Rev. B*, vol. 85, 2012, 081405(R).

[77] A. Yu. Nikitin, F. Guinea, F. J. Garcia-Vidal, and L. Martin-Moreno, "Edge and waveguide terahertz surface plasmon modes in graphene microribbons," *Phys. Rev. B*, vol. 84, 2011, 161407(R).

[78] L. Brey and H. A. Fertig, "Elementary electronic excitations in graphene nanoribbons," *Phys. Rev. B*, vol. 75, 2007, 125434.

[79] D. R. Anderson and H. Raza, "Plasmon dispersion in semimetallic armchair graphene nanoribbons," *Phys. Rev. B*, vol. 85, 2012, 075425.

[80] V. V. Popov, T. Yu. Bagaeva, T. Otsuji, and V. Ryzhii, "Oblique terahertz plasmons in graphene nanoribbon arrays," *Phys. Rev. B*, vol. 81, 2010, 073404.

[81] M. Y. Han, B. Ozyilmaz, Y. Zhang, and P. Kim, "Energy band-gap engineering of graphene nanoribbons," *Phys. Rev. Lett.*, vol. 98, 2007, 206805.

[82] S. Thongrattanasiri, A. Manjavacas, and F. J. Garcia de Abajo, "Quantum finite-size effects in graphene plasmons," *ACS Nano*, vol. 6, pp. 1766–1775, 2012.

[83] C. Cocchi, D. Prezzi, A. Ruini, E. Benassi, M. J. Caldas, S. Corni, and E. Molinari, "Optical excitations and field enhancement in short graphene nanoribbons," *J. Phys. Chem. Lett.*, vol. 3, pp. 924–929, 2012.

[84] R. A. Muniz, H. P. Dahal, A. V. Balatsky, and S. Haas, "Impurity-assisted nanoscale localization of plasmonic excitations in graphene," *Phys. Rev. B*, vol. 82, 2010, 081411(R).

[85] M. H. Gass, U. Bangert, A. L. Bleloch, P. Wang, R. R. Nair, and A. K. Geim, "Free-standing graphene at atomic resolution," *Nature Nanotechnol.*, vol. 3, pp. 676–681, 2008.

[86] J. Bardeen, L. N. Cooper, and J. R. Schrieffer, "Theory of superconductivity," *Phys. Rev.*, vol. 108, pp. 1175–1204, 1957.

[87] D. C. Tsui, H. L. Stormer, and A. C. Gossard, "Two-dimensional magnetotransport in the extreme quantum limit," *Phys. Rev. Lett.*, vol. 48, pp. 1559–1562, 1982.

[88] R. B. Laughlin, "Anomalous quantum hall effect: An incompressible quantum fluid with fractionally charged excitations," *Phys. Rev. Lett.*, vol. 50, pp. 1395–1398, 1983.

[89] A. Bostwick, F. Speck, T. Seyller, K. Horn, M. Polini, R. Asgari, A. H. MacDonald, and E. Rotenberg, "Observation of plasmarons in quasi-freestanding doped graphene," *Science*, vol. 328, pp. 999–1002, 2010.

[90] H. Yan, T. Low, W. Zhu, Y. Wu, M. Freitag, X. Li, F. Guinea, P. Avouris, and F. Xia, "Damping pathways of mid-infrared plasmons in graphene nanostructures," *Nature Photon.*, vol. 7, pp. 394–399, 2013.

[91] H. Buljan, M. Jablan, and M. Soljačić, "Graphene plasmonics: Damping of plasmons in graphene," *Nature Photon.*, vol. 7, pp. 346–348, 2013.

[92] Z. Fang, S. Thongrattanasiri, A. Schlater, Z. Liu, L. Ma, Y. Wang, P. M. Ajayan, P. Nordlander, N. J. Halas, and F. J. Garcia de Abajo, "Gated tunability and hybridization of localized plasmons in nanostructured graphene," *ACS Nano*, vol. 7, pp. 2388–2395, 2013.

[93] P. B. Johnson and R. W. Christy, "Optical constants of noble metals," *Phys. Rev. B*, vol. 6, pp. 4370–4379, 1972.

[94] T. Holstein, "Optical and infrared volume absorptivity of metals," *Phys. Rev.*, vol. 96, pp. 535–536, 1954.

[95] S. Das Sarma, S. Adam, E. H. Hwang, and E. Rossi, "Electronic transport in two-dimensional graphene," *Rev. Mod. Phys.*, vol. 83, pp. 407–470, 2011.

[96] A. K. M. Newaz, Y. S. Puzyrev, B. Wang, S. T. Pantelides, and K. I. Bolotin, "Probing charge scattering mechanisms in suspended graphene by varying its dielectric environment," *Nature Commun.*, vol. 3, 2012, 734.

[97] K. I. Bolotin, K. J. Sikes, J. Hone, H. L. Stormer, and P. Kim, "Temperature-dependent transport in suspended graphene," *Phys. Rev. Lett.*, vol. 101, 2008, 096802.

[98] N. M. R. Peres, R. M. Ribeiro, and A. H. Castro Neto, "Excitonic effects in the optical conductivity of gated graphene," *Phys. Rev. Lett.*, vol. 105, 2008, 055501.

[99] A. G. Grushin, B. Valenzuel, and M. A. H. Vozmediano, "Effect of Coulomb interactions on the optical properties of doped graphene," *Phys. Rev. B*, vol. 80, 2009, 155417.

[100] P. Tassin, T. Koschny, M. Kafesaki, and C. M. Soukoulis, "A comparison of graphene, superconductors and metals as conductors for metamaterials and plasmonics," *Nature Photon.*, vol. 6, pp. 259–264, 2012.

[101] O. Ilic, M. Jablan, J. D. Joannopoulos, I. Celanovic, H. Buljan, and M. Soljacic, "Near-field thermal radiation transfer controlled by plasmons in graphene," *Phys. Rev. B*, vol. 85, 2012, 155422.

[102] O. Ilic, M. Jablan, J. D. Joannopoulos, I. Celanovic, and M. Soljacic, "Overcoming the black body limit in plasmonic and graphene near-field thermophotovoltaic systems," *Opt. Exp.*, vol. 20, 2012, A366.

ABOUT THE AUTHORS

Marinko Jablan received the B.Sc. and Ph.D. degrees in physics from the University of Zagreb, Zagreb, Croatia, in 2006 and 2012, respectively.

He was a visiting student at the Massachusetts Institute of Technology (MIT), Cambridge, MA, USA, for one year during his Ph.D. studies as part of an exchange program. In 2011, he was a Principal Investigator of a research project "Exploiting optomechanical properties of graphene for novel nanotechnologies," funded by the Unity through Knowledge Fund in Croatia.

Dr. Jablan won the Science Award in 2008, awarded annually by the Croatian Science Foundation to one student in natural sciences. He won the Top Scholarship for students in 2006.

Marin Soljačić received the B.S.E. degree in physics and the B.S.E. degree in electrical engineering from the Massachusetts Institute of Technology (MIT), Cambridge, MA, USA, in 1996 and the Ph.D. degree in physics from Princeton University, Princeton, NJ, USA, in 2000.

In September 2000, he was named an MIT Pappalardo Fellow in Physics, and in 2003, he was appointed as a Principal Research Scientist in the Research Laboratory of Electronics at MIT. In September 2005, he became an Assistant Professor of Physics at MIT; in July 2010, an Associate Professor of Physics at MIT; and in July 2011, a Full Professor of Physics.

Dr. Soljačić is the recipient of the Adolph Lomb medal from the Optical Society of America (2005), and the TR35 award of the *Technology Review* magazine (2006). In 2008, he was awarded a MacArthur fellowship grant. He has been a correspondent member of the Croatian Academy of Engineering since 2009. In 2011, he became a Young Global Leader (YGL) of the World Economic Forum.

Hrvoje Buljan received the M.Sc. degree and the Ph.D. degree in physics from the University of Zagreb, Zagreb, Croatia, in 1997 and 2002, respectively.

In 2002–2004, he was a Postdoctoral Fellow at the Technion—Israel Institute of Technology, Haifa, Israel. His research at the time was focused on nonlinear optical phenomena. After this period, he moved back to the University of Zagreb as an Assistant Professor and formed his group with activities also in ultracold atomic gases and in recent years plasmons in graphene. He has been an Associate Professor of Physics at the University of Zagreb since 2009.

Dr. Buljan received the Annual Croatian State Award for Science in 2010.